Quantum holography with biphotons of high Schmidt number

Fabrice Devaux,[1,*] Alexis Mosset,[1] Florent Bassignot,[2] and Eric Lantz[1]

[1]*Département d'Optique P. M. Duffieux, Institut FEMTO-ST, UMR No. 6174, CNRS, Université Bourgogne Franche-Comté, 15b Avenue des Montboucons, 25030 Besançon, France*

[2]*FEMTO Engineering, 15b Avenue des Montboucons, 25030 Besançon, France*

(Received 1 May 2018; published 27 March 2019)

We report the results of two-photon quantum holography where spatial information stored in phase holograms is retrieved by measuring quantum spatial correlations between two images formed by spatially entangled twin photons with a Schmidt number of 450 in the two-dimensional transverse space. In our experiments, the entire flux of spontaneous down-converted photons illuminates the phase holograms and the photons of signal-idler pairs transmitted by the holograms are detected separately in the far field on two electron-multiplying charge coupled device cameras.

DOI: 10.1103/PhysRevA.99.033854

I. INTRODUCTION

High-dimensionality spatial entanglement allows access to large Hilbert spaces, with applications in numerous fields of quantum optics such as quantum lithography [1], quantum computation [2], and quantum ghost imaging [3]. By itself, a source of quantum light issued from spontaneous down-conversion (SPDC) appears as incoherent, preventing the formation of an image of the spatial spectrum of an object (a transparency) in the Fourier plane. However, coincidence imaging of the pairs of twin photons allows this spatial spectrum to be retrieved, as demonstrated in experiments such as demonstration of spatial antibunching [4], observation of two-photon speckle patterns [5], transfer of the angular spectrum of the transparency modulating the pump beam [6], and ghost imaging of a pure phase object [7]. All these experiments measured coincidences between two single-photon-counting modules scanned on the signal and idler images. These procedures are time consuming, even if improved by compressive sensing [8], and use a very small number of the incident photons, leading to potential loopholes [9] if applied to the demonstration of basics properties of entanglement like the Einstein-Podolsky-Rosen (EPR) paradox [10].

Because of these drawbacks, imaging with single-photon sensitive cameras has became more and more popular and allows massively parallel coincidence counting. Examples of experiments include sub-shot-noise imaging [11,12] using a low-noise CCD camera, demonstration of a high degree of EPR paradox [13] and of transmission of biphotons through a nonunitary object [14] using electron-multiplying CCD (EMCCD) cameras, unity contrast EPR-based ghost imaging with an intensified CCD camera [15], and holography of a single photon with an intensified complementary metal-oxide semiconductor camera [16].

In this paper we report coincidence imaging of bidimensional phase holograms using two EMCCD cameras. Unlike in ghost imaging experiments, the phase of the hologram is imprinted on both photons, ensuring direct coherent manipulation of the biphoton function for the two spatial dimensions: holography becomes quantum for images with a high number of degrees of freedom. As in Refs. [4,5], no single-photon image is formed in the Fourier plane, while the cross correlation of the images allows a coherent image to be retrieved in the far field, with an equivalent wavelength equal to half the signal or idler wavelength, as in [17]. Very recently, a spatial light modulator was used to structure a SPDC light beam and obtain coincidence imaging with a single EMCCD camera [18]. In the latter experiment, both photons of a pair are degenerate (same frequency and polarization), while in our experiment the twin photons are cross polarized, allowing the detection of two distinct images on two cameras: we present in the following the measurement of the second-order correlation directly connected to the biphoton amplitude, but correlations of all orders can in principle be detected and all further coherent manipulations are possible, on either one or both photons.

II. THEORY AND HYPOTHESES

For a sufficiently thin crystal, it can be assumed that the two photons of a pair are created at the same random place. This assumption is equivalent to neglecting the uncertainty in the image plane due to phase-matching conditions. Hence, the two-photon spectral wave function of SPDC emitted from a thin crystal pumped by a monochromatic beam of angular frequency ω_p and of amplitude $E_p(\mathbf{r})$ is given by [19]

$$\psi(\mathbf{r}_1,\mathbf{r}_2;\omega_s) \propto \int E_p(\mathbf{r}) h_s(\mathbf{r}_1,\mathbf{r};\omega_s) h_i(\mathbf{r}_2,\mathbf{r};\omega_p-\omega_s) d\mathbf{r}, \tag{1}$$

where $\mathbf{r}_1$ and $\mathbf{r}_2$ are transverse positions in the plane of separate detectors (EMCCD_1 for the signal and EMCCD_2 for the idler), $\mathbf{r}$ is a coordinate in the image plane of the crystal where the hologram lies, and $h_s(\mathbf{r}_1,\mathbf{r};\omega_s)$ and $h_i(\mathbf{r}_2,\mathbf{r};\omega_p-\omega_s)$ are

*Corresponding author: fabrice.devaux@univ-fcomte.fr

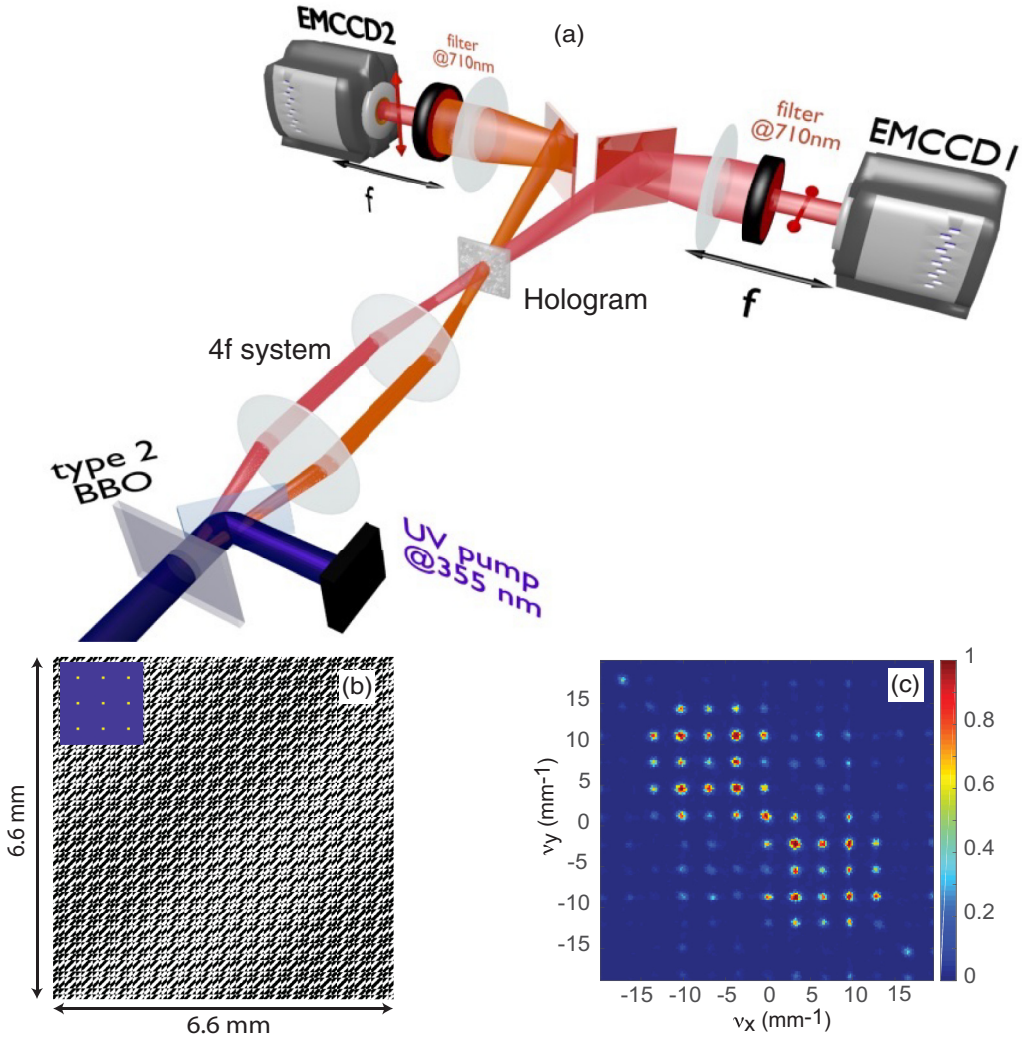

FIG. 1. (a) Experimental setup: Twin photon pairs at 710 nm are generated by SPDC in a type-II BBO crystal. The crystal is imaged with a 4-f optical system on a binary phase hologram engraved on a glass slide. The photon's signal and idler transmitted by the hologram are then naturally separated by free space propagation due to the walk-off. They are then detected and resolved spatially in the far field on two EMCCD cameras used in photon-counting mode. (b) Pattern of the $(0-\frac{\pi}{2})$ binary phase hologram. The inset represents the pattern encoded in the hologram: an array of nine Dirac peaks. (c) Restitution of the same hologram designed for a coherent illumination at 710 nm. By comparing it to the encoded pattern, the additional periodically distributed peaks are due to the binary character of the hologram.

the impulse response functions of the separate linear imaging systems for the signal and the idler beams, respectively.

Now let $t(\mathbf{r}) = e^{i\varphi(\mathbf{r})}$ be the transmission of the phase hologram with a phase modulation $\varphi(\mathbf{r})$ and let us make some assumptions. First, we assume that the hologram is thin and planar. Second, the binary phase hologram is designed in such a way that the ± 1 diffraction orders are centered, in a far field, on ± 6-mm^{-1} spatial frequencies which are much smaller than the 64-mm^{-1} phase-matching bandwidth (FWHM) of the type-II β barium borate (BBO) crystal (see the the first paragraph in Sec. III dedicated to the experimental setup), in agreement with the above assumption of neglecting the effect of imperfect phase matching. Moreover, because SPDC is detected in a narrow band around degeneracy, the biphoton state is assumed to be monochromatic ($\omega_i = \omega_p - \omega_s = \omega_s$). Third, in our experimental setup [Fig. 1(a)], as the hologram is placed in the near field of the crystal and because all photons are collected by the 4-f imaging system, in Eq. (1), we can consider that the separate optical systems are formed only by the hologram and the two identical Fourier transform optical systems (2-f systems). Then the impulse responses are given by

$$h_{s,i}(\mathbf{r}_{1,2}, \mathbf{r}; \omega) = t_{s,i}(\mathbf{r}) \frac{e^{-2ikf}}{i\lambda f} e^{-(ik/f)\mathbf{r}_{1,2}\mathbf{r}}, \tag{2}$$

where k and λ are the signal or idler wave number and wavelength (at the degeneracy $k_s = k_i = k$ and $\lambda_s = \lambda_i = \lambda$). Then Eq. (1) becomes

$$\psi(\mathbf{r}_1, \mathbf{r}_2) \propto \int E_p(\mathbf{r}) t_s(\mathbf{r}) t_i(\mathbf{r}) e^{-(ik/f)(\mathbf{r}_1+\mathbf{r}_2)\mathbf{r}} d\mathbf{r}. \tag{3}$$

Because $t_s(\mathbf{r}) = t_i(\mathbf{r}) = t(\mathbf{r})$, the experimental two-photon coincidence rate at two positions in the separate detection planes

is given by

$$G^{(2)}(\mathbf{r}_1,\mathbf{r}_2)=|\psi(\mathbf{r}_1,\mathbf{r}_2)|^2\propto\left|\widetilde{E}_p\left(\frac{\mathbf{r}_1+\mathbf{r}_2}{\lambda f}\right)*\widetilde{t}^2\left(\frac{\mathbf{r}_1+\mathbf{r}_2}{\lambda f}\right)\right|^2, \tag{4}$$

where $*$ denotes the convolution product and the tilde the bidimensional Fourier-transform operator. In this expression, the transmission of the hologram is squared, unlike in classical coherent imaging. In consequence, while binary phase holograms are usually designed with a $(0-\pi)$ phase step for efficient restitution with coherent light, a $(0-\frac{\pi}{2})$ phase step must be engraved when a biphoton source is used or, equivalently, the $(0-\pi)$ phase step must be engraved by considering a halved wavelength [17].

III. EXPERIMENTS AND RESULTS

The experimental setup is illustrated in Fig. 1(a). Photon pairs are generated via SPDC in a type-II geometry in a 0.8-mm-long BBO crystal pumped at 355 nm. The pump pulses are provided by a passively-Q-switched Nd:YAG laser (330-ps pulse duration, 27-mW mean power, 1-kHz repetition rate, and 1.6-mm FWHM beam diameter). The crystal (i.e., near field of twin photons) is imaged with a 4-f imaging system on a binary phase hologram with a transversal and an angular magnification of -1 and the entire flux of spontaneously down-converted light illuminates the hologram. Figure 1(b) shows the binary pattern engraved on a glass slide to create the phase hologram and the insert corresponds to the pattern encoded in the hologram: an array of nine Dirac peaks. The phase holograms are designed to produce off-axis patterns and the binary hologram, i.e., diffractive optical elements (DOEs) [20], gives a restitution of the original pattern at ±1 diffraction orders. The engraving depth of the holograms is adjusted to produce a $(0-\frac{\pi}{2})$ binary phase modulation at 710 nm in order to optimize the diffraction efficiency of the hologram with the biphotons source. The cross-polarized signal and idler beams transmitted by the hologram are then naturally separated by free space propagation due to the walk-off. Finally, photons of pairs are detected and resolved spatially in the far field on two EMCCD cameras (Andor iXon3) used in photon-counting mode [21]. Before detection, photons pairs emitted around the degeneracy are selected by narrow-band interference filters centered at 710 nm ($\Delta\lambda \backsimeq 4$ nm). The vertical and horizontal red arrows symbolize the polarization directions of the signal and idler beams.

The protocol for measuring spatial momentum correlations between twin images is the same as the one we proposed for measuring the EPR paradox [13,22] and temporal ghost imaging [23] with twin images. For a set of twin images, we apply a thresholding procedure to convert the grayscales into binary values that correspond to one or zero photons. Then a spatial coincidence correlation function is obtained by calculating the normalized cross correlation of photodetection images, after subtraction from these images of their deterministic part (i.e., the mean of the images).

First, the hologram is removed from the experimental setup. From the normalized cross correlation in momentum calculated with a set of 100 twin images [Fig. 2(a)], we measure the width of the correlation peak, expressed in standard deviations, which gives, in spatial frequency units, $\sigma_{\nu_x}=0.69\ \mathrm{mm}^{-1}$ and $\sigma_{\nu_y}=0.59\ \mathrm{mm}^{-1}$. With $\sigma_\phi=27\ \mathrm{mm}^{-1}$ the standard deviation deduced from the 64-mm^{-1} FWHM of the phase-matching function [Fig. 2(c)], we can estimate roughly the whole dimensionality V, i.e., the Schmidt number of the biphoton wave function in the two-dimensional transverse space. As stated in [24], the Schmidt number is given, in our situation of strong entanglement dominated by anticorrelation of the wave vectors, by

$$V=\frac{\sigma_\phi^2}{4\sigma_{\nu_x}\sigma_{\nu_y}}\approx 450. \tag{5}$$

Note that this value is given by Gaussian fittings and that a proper consideration of the sinc nature of the transfer function due to phase matching results in a higher value [24]. This experimental result has to be compared with the theoretical value given by [25]

$$V_{\mathrm{th}}=\left(\frac{2\pi 0.69}{1.89}\right)^2\frac{\sigma_{\mathrm{pump}}^2}{\lambda_s L\left(n_s^{-1}+n_i^{-1}\right)}\approx 3500, \tag{6}$$

where L is the crystal thickness, $\sigma_{\mathrm{pump}}\approx 0.68$ mm is the standard deviation deduced from the FWHM of the Gaussian pump beam, and n_s and n_i are the refractive indices of the BBO crystal. The difference between these two values comes mainly from the enlargement of the correlation peak due to the bandwidth of the interferential filters, giving an inexactly monochromatic SPDC (see [25] for more details), and also from the 4-f imaging system inducing some geometric aberrations. The experimental value remains very high, allowing coincidence imaging of quite complex objects.

We also calculated the integral of the normalized correlation peak, i.e., the degree of correlation, that is equal to 0.25. This value represents the ratio between the number of photons detected in pairs and the total number of photons. This result is also consistent with the equivalent quantum efficiency of the entire detection system which includes the quantum efficiency of the cameras and the transmission coefficients of the various optical components (filters, lenses, and dichroic mirrors) [22]. Finally, we verified that there is no deterministic correlation between images that do not share pump pulses [Fig. 2(b)]. We now put the phase hologram back into the experimental setup. In Fig. 2(c), which shows the far-field mean spatial distribution of photons signal (or idler) transmitted by the hologram, we can observe that the spatial information encoded in the hologram is not retrieved, because of the incoherent nature of SPDC [5,6]. In contrast, and in good agreement with Eq. (4), when cross correlation in momentum between twin images is calculated, the spatial distribution of the two-photon coincidence rate exhibits a pattern [Fig. 2(d)] which appears at the ±1 diffraction orders the original pattern encoded in the hologram: an array of nine Dirac peaks (in white dotted squares). As for coherent illumination [Fig. 1(c)], some additional periodically distributed peaks are also visible due to the binary character of the hologram. In order to improve the signal-to-noise ratio (SNR) of the retrieved pattern, this cross-correlation image is calculated over 80 000 twin images. Although the engraving depth of the hologram is adjusted with an accuracy of about 10% to give a $(0-\frac{\pi}{2})$ phase step, the correlation peak corresponding the zeroth-order diffraction of

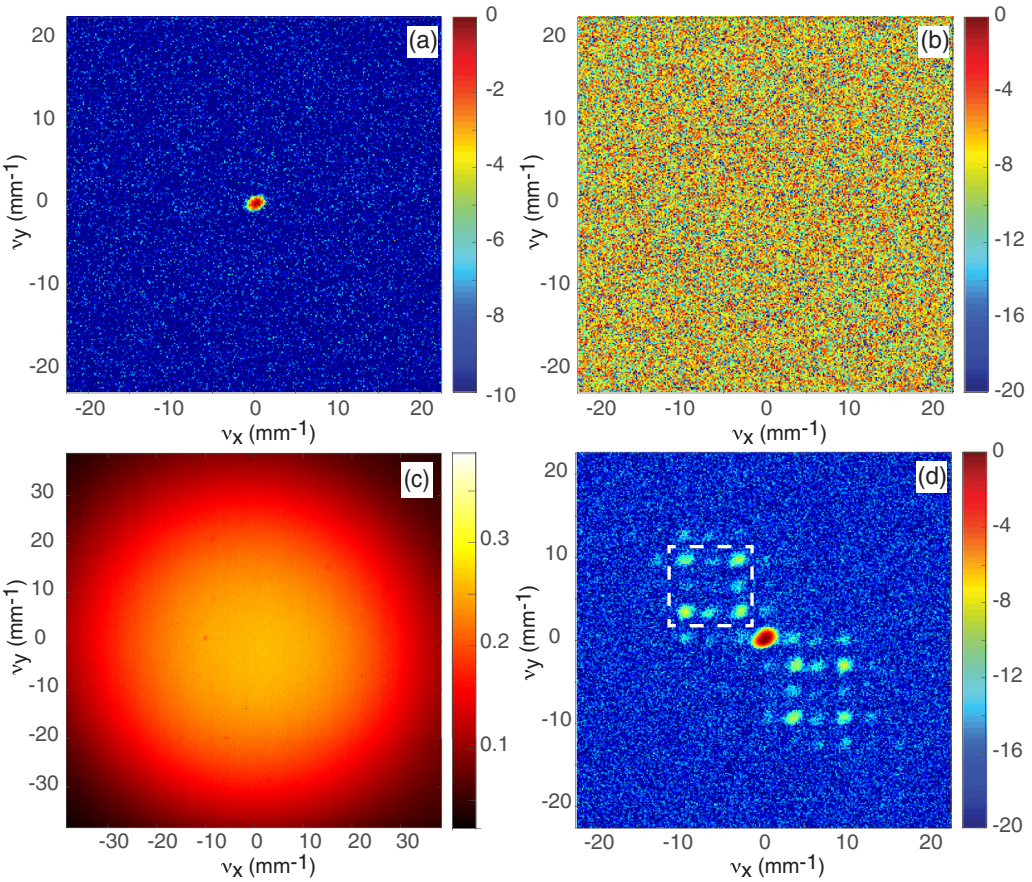

FIG. 2. Without the hologram, in dB, (a) normalized cross correlation in momentum between 100 twin images and (b) images that do not share pump pulses, and with the hologram, (c) average photon number in single far-field images (signal or idler) of SPDC and (d) restored hologram formed by the normalized cross correlation in momentum, given in dB, calculated over 80 000 twin images. The white dashed square indicates the location of the original pattern encoded in the hologram.

the hologram is much more intense than the ± 1 diffraction orders, unlike in the restored hologram obtained with a coherent illumination at 710 nm [Fig. 1(c)]. From the integral of the whole normalized correlation pattern, the degree of correlation of twin images is estimated to 0.20. This is smaller than the degree of correlation measured without the hologram because the transverse momenta of some photon pairs transmitted by the hologram are greater than the maximum sampling spatial frequency imposed by the sensor dimensions. The results presented here correspond to the best position of the hologram, minimizing the level of the correlation peak at the zeroth-order diffraction.

To explain the large amplitude of the zeroth-order correlation peak, we evaluated the impact of geometric aberrations of the imaging system between the crystal and the hologram plane using ray tracing software. Indeed, because of the walk-off ($\sim 6.5^\circ$), the rotation symmetry around the optical axis of the imaging system is not respected. Moreover, the off-axis propagation of the twin photons makes the paraxial approximation no longer valid. Using ray tracing software, we generated twin rays coming, for each couple, from a unique point chosen randomly in the crystal and propagating in symmetrical directions (one corrected from the walk-off), chosen randomly in the angular range allowed by phase matching. For a large number of realizations, we calculated the average distance between the twin rays at the intersection of an image plane symbolizing the position of the hologram. Finally, we adjusted the position of this plane to minimize this average distance. For parameters corresponding to the experimental conditions (crystal dimensions, shape of the lenses, etc.) and for the best position of the image plane, we obtained an average distance approximately equal to 70 μm in the transverse plane, which is larger than the size of a pixel of the hologram (~ 13 μm). This distance also corresponds to a defocusing in the longitudinal direction of approximately ± 0.6 mm. Since this defocusing is underestimated (because additional experimental aberrations would have to be taken into account. e.g., various tiny misalignments, geometric aberrations introduced by filters and the dichroic mirror, etc.), we can conclude that, in practice, twin photons are not transmitted at the same place and with the same phase. It results that, although Eq. (1) remains valid, the impulse responses are no longer given by Eq. (2). Indeed, the effect of the hologram transmission on the Green's function $h_s(\mathbf{r_1}, \mathbf{r}'; \omega)$ cannot be taken into account by a simple multiplication since a crystal coordinate r' no longer corresponds to an hologram coordinate. A formalism involving for each beam two impulse responses (one from the crystal to the hologram and one from the hologram to the camera) could be developed [26], leading to double integrals which must be calculated for each couple of pixels $(\mathbf{r}_1, \mathbf{r}_2)$.

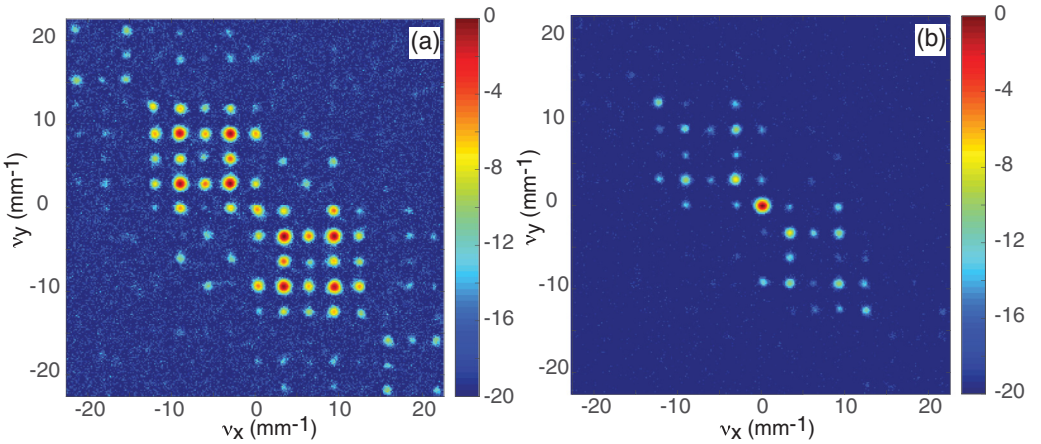

FIG. 3. Normalized averaged cross correlation of images issued from stochastic simulations, sampled and scaled for direct comparison with the experimental results of Fig. 2(d), with (a) no defocusing and (b) 1.5-mm defocusing.

For a bidimensional image, the computation time would scale at the eighth power of the number of pixels in one dimension, which is prohibitively long. Fortunately, stochastic simulations based on the Wigner formalism [27] allow here accurate results, reproducing, when repeated several thousand times and averaged, all specific quantum features like greater correlations with twin pixels than with adjacent ones in both the direct and the reciprocal space: characterization of phenomena like the EPR paradox is possible [13]. Figure 3(a) shows the cross-correlation image for no defocusing, which appears to be in good agreement with the coherent restitution of the hologram [Fig. 1(c)] but quite different of the experimental image [Fig. 2(d)]. On the other hand, introducing 1.5 mm of defocusing leads to a simulated image [Fig. 3(b)] very close of the experimental one. Note that these simulations also take into account the propagation in the crystal, resulting, for the

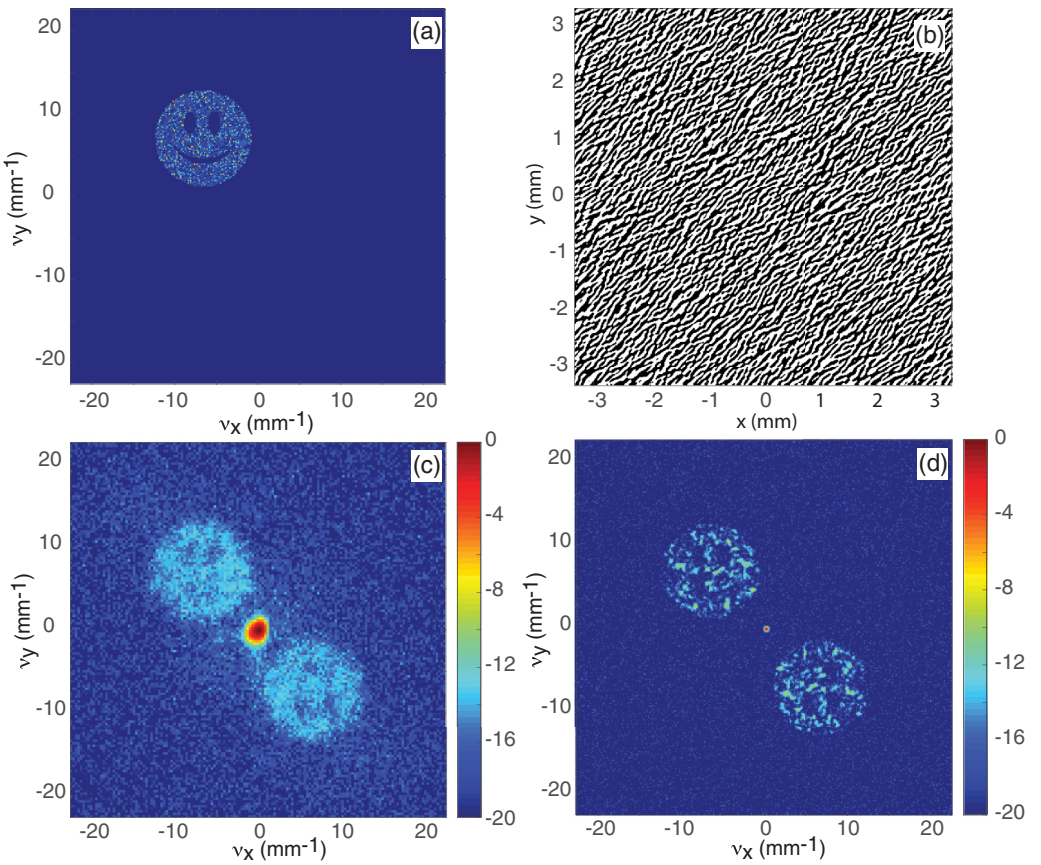

FIG. 4. (a) Picture encoded in the DOE: a 10-mm^{-1}-diam smiley face modulated by a deterministic speckle pattern. (b) Binary pattern of the DOE. (c) Restored hologram formed by the normalized cross correlation calculated over 270 000 twin images. (d) Normalized averaged cross correlation of images issued from 10 000 stochastic simulations where no defocusing is considered.

mean one-photon image, in a phase-matching cone in good agreement with Fig. 2(c).

Finally, we used an another DOE [Fig. 4(b)] designed to produce a smiley face of 10 mm^{-1} diameter modulated by a deterministic speckle pattern [Fig. 4(a)]. Figures 4(c) and 4(d) show for comparison the restored hologram formed by the normalized cross correlation calculated over 270 000 twin images and the normalized averaged cross correlation of images issued from 10 000 stochastic simulations where no defocusing is considered, respectively. Although spatial coincidences reproduce the original pattern, we can observe that the resolution of the smiley face is strongly limited by the size of the speckle grains that compose it. Indeed, according to Eq. (4), these grains are the result of the convolution between the speckle grains of the initial pattern and the intercorrelation peak observed at the zeroth-order diffraction, of width proportional to the inverse of the width of the pump beam in the near field. From the integral of the whole normalized correlation pattern, the degree of correlation of twin images is estimated to 0.25. Because coincidences between twin photons are spread over large areas, it is necessary to cumulate a much larger number of realizations in order that the pattern formed by the coincidences emerges from the background noise. For the same reason as with the previous hologram, we can observe that the zeroth-order diffraction peak concentrates a significative number of the spatial coincidences between the twin images.

IV. CONCLUSION

To summarize, we have shown that two-photon imaging potentially allows coherent manipulation of light in complex situations like holography. As quoted from [7], phase objects are of special interest in quantum information processing since they introduce a unitary operation that is reversible (in contrast to amplitude masks of any form). These results generalize previous demonstrations where the biphoton image was a one-dimensional interference pattern created by a double slit [4] or a one-dimensional speckle scattered by a rough surface [5]. Unlike these previous experiments, all the light is used, preventing the part of the fair-sampling loophole that is due to the selection of the small number of photons that are in coincidence and allowing full bidimensional manipulation of biphoton states with high Schmidt number, with potential applications in current hot topics, such as boson sampling [28]. As a final remark, equivalent schemes are probably feasible with classical light. Indeed, the experiment described in this paper does not involve specific quantum properties, for example, the sub-Poissonian character of the image difference [13]: Here, only the phase-sensitive character of the correlation between twin beams is used [29]. Several years ago, a ghost image of an amplitude object was obtained by using a pair of programmable spatial light modulators to impose anticorrelated random phases on the reference and signal beams [30]. Such an experiment could probably be transposed to coincidence imaging of a hologram, with probably a lower SNR than with twin beams [29]. The scheme does not appear simpler than the present one and amplified quantum noise appears as a reliable source to perform coincidence holography.

ACKNOWLEDGMENTS

This work was partly supported by the French "Investissements d'Avenir" program, Project ISITE-BFC (Contract No. ANR-15-IDEX-03) and the RENATECH network and its FEMTO-ST MIMENTO technological facility.

[1] A. N. Boto, P. Kok, D. S. Abrams, S. L. Braunstein, C. P. Williams, and J. P. Dowling, Phys. Rev. Lett. **85**, 2733 (2000).
[2] D. S. Tasca, R. M. Gomes, F. Toscano, P. H. Souto Ribeiro, and S. P. Walborn, Phys. Rev. A **83**, 052325 (2011).
[3] T. B. Pittman, Y. H. Shih, D. V. Strekalov, and A. V. Sergienko, Phys. Rev. A **52**, R3429 (1995).
[4] W. A. T. Nogueira, S. P. Walborn, S. Pãdua, and C. H. Monken, Phys. Rev. Lett. **86**, 4009 (2001).
[5] W. H. Peeters, J. J. D. Moerman, and M. P. van Exter, Phys. Rev. Lett. **104**, 173601 (2010).
[6] C. H. Monken, P. H. Souto Ribeiro, and S. Pãdua, Phys. Rev. A **57**, 3123 (1998).
[7] A. F. Abouraddy, P. R. Stone, A. V. Sergienko, B. E. A. Saleh, and M. C. Teich, Phys. Rev. Lett. **93**, 213903 (2004).
[8] G. A. Howland and J. C. Howell, Phys. Rev. X **3**, 011013 (2013).
[9] E. Lantz, P.-A. Moreau, and F. Devaux, Phys. Rev. A **90**, 063811 (2014).
[10] J. C. Howell, R. S. Bennink, S. J. Bentley, and R. W. Boyd, Phys. Rev. Lett. **92**, 210403 (2004).
[11] O. Jedrkiewicz, Y.-K. Jiang, E. Brambilla, A. Gatti, M. Bache, L. A. Lugiato, and P. Di Trapani, Phys. Rev. Lett. **93**, 243601 (2004).
[12] G. Brida, M. Genovese, and I. R. Berchera, Nat. Photon. **4**, 227 (2010).
[13] P.-A. Moreau, F. Devaux, and E. Lantz, Phys. Rev. Lett. **113**, 160401 (2014).
[14] M. Reichert, H. Defienne, X. Sun, and J. W. Fleischer, J. Opt. **19**, 044004 (2017).
[15] R. S. Aspden, D. S. Tasca, R. W. Boyd, and M. J. Padgett, New J. Phys. **15**, 073032 (2013).
[16] R. Chrapkiewicz, M. Jachura, K. Banaszek, and W. Wasilewski, Nat. Photon. **10**, 576 (2016).
[17] I. F. Santos, M. A. Sagioro, C. H. Monken, and S. Pãdua, Phys. Rev. A **67**, 033812 (2003).
[18] H. Defienne, M. Reichert, and J. W. Fleischer, Phys. Rev. Lett. **121**, 233601 (2018).
[19] B. E. A. Saleh, A. F. Abouraddy, A. V. Sergienko, and M. C. Teich, Phys. Rev. A **62**, 043816 (2000).
[20] D. C. O'Shea, T. J. Suleski, A. D. Kathman, and D. W. Prather, *Diffractive Optics* (SPIE, Bellingham, 2003).
[21] E. Lantz, J.-L. Blanchet, L. Furfaro, and F. Devaux, Mon. Not. R. Astron. Soc. **386**, 2262 (2008).
[22] E. Lantz, S. Denis, P.-A. Moreau, and F. Devaux, Opt. Express **23**, 26472 (2015).

[23] S. Denis, P.-A. Moreau, F. Devaux, and E. Lantz, J. Opt. **19**, 034002 (2017).
[24] C. K. Law and J. H. Eberly, Phys. Rev. Lett. **92**, 127903 (2004).
[25] F. Devaux, J. Mougin-Sisini, P. A. Moreau, and E. Lantz, Eur. Phys. J. D **66**, 192 (2012).
[26] A. F. Abouraddy, B. E. A. Saleh, A. V. Sergienko, and M. C. Teich, J. Opt. Soc. Am. B **19**, 1174 (2002).
[27] E. Lantz, N. Treps, C. Fabre, and E. Brambilla, Eur. Phys. J. D **29**, 437 (2004).
[28] H. Defienne, M. Barbieri, I. A. Walmsley, B. J. Smith, and S. Gigan, Sci. Adv. **2**, e1501054 (2016).
[29] B. I. Erkmen and J. H. Shapiro, Adv. Opt. Photon. **2**, 405 (2010).
[30] D. Venkatraman, N. D. Hardy, F. N. C. Wong, and J. H. Shapiro, Opt. Lett. **36**, 3684 (2011).